Heat and Mass Transfer in Water-Laden Sandstone: Microwave Heating

Our previous theoretical model was extended to predict the heat and mass transfer phenomena in microwave-heated porous materials. A water-filled sandstone was heated in microwaves and its drying rates and temperature profiles were measured. Predictions agree well with observations. Besides moisture loss rates and temperature profiles, the model also predicts local moisture content, gas densities, and pressure. These latter quantities were not measured in our work, but are of interest since they reveal the basic mechanisms of heat and mass transfer in internally heated porous media.

CHEN KOU WEI
and H. T. DAVIS

Department of Chemical Engineering and Materials Science
University of Minnesota
Minneapolis, MN 55455

and

E. A. DAVIS
and JOAN GORDON

Department of Food Science and Nutrition
University of Minnesota
St. Paul, MN 55108

SCOPE

Microwave heating is an important technique in industrial drying and food processing because it has several advantages over convective heating, specific advantages being fast heating, high energy efficiency, and uniform moisture distribution in products. Local temperatures, moisture content, and pressure within a wet porous material heated by microwaves have been measured (Lyons and Hatcher, 1972), but the dynamic phenomena remain little studied. By incorporation of Lambert's law for the attenuation of microwave power in dielectric media, we solved our previous mathematical model (Wei et al., 1984) to predict the fluid flow and heat transfer phenomena in a microwave-heated, water-laden sandstone.

CONCLUSIONS AND SIGNIFICANCE

The predicted phenomena are shown in Figures 4-12. In contrast to the convectively heated sample we studied earlier (1984), the microwave-heated sample is hotter inside, the liquid volume fraction increases slightly toward the sample surface, and the vapor density decreases to the surface and increases with time. Except for a short time during which it has a weak maximum, the air density increases toward the surface and decreases with time. A pressure maximum builds up in the sample before it starts falling to nearly atmospheric pressure. During most of the heating period, air slowly flows to the sample's center, water vapor flows to the surface, and liquid vaporizes as its flows to the surface with higher flux than vapor.

The results described here help understand the pore-level transport phenomena when a porous medium is heated internally. The model, having been successful in predicting moisture loss rates and temperature profiles in water-laden sandstone heated by both convection and microwave sources, should provide a credible theoretical tool for design of optimal combinations of convective and microwave heating for drying and cooking, although sample shrink is a complication accompanying cooking foods not encountered in heating sandstone.

INTRODUCTION

Drying is often a limiting step in the manufacture of industrial products, so it is important to understand the drying mechanisms. There are two drying methods in common use: convective heating and microwave heating. Microwave heating offers several distinct advantages over convective heating, for example, fast heating, high energy efficiency, and uniform moisture distribution in products., although the nonuniform heating intensity in microwave fields needs to be improved (Watanabe et al., 1978).

Lyons and Hatcher (1972) measured the temperature, moisture content, and pressure profiles in wet cotton dried by microwaves. They found that near the surface, the temperature decreases sharply in the radial direction, that moisture spreads evenly throughout the sample, and that a central pressure peak rises in the beginning and drops afterward. These profiles are quite different from those predicted in convective heating (Wei et al., 1984).

In order to understand the heat and mass transfer mechanisms in microwave-heated, fluid-filled porous materials, we investigated experimentally the progressive temperature distribution and water

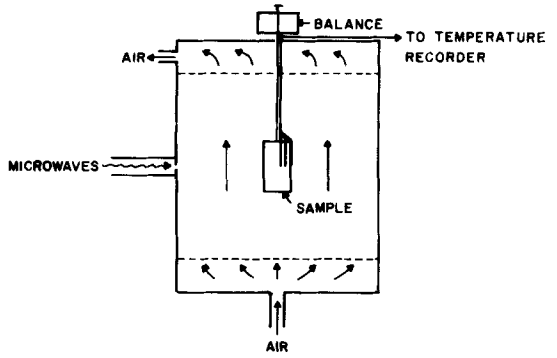

Figure 1. A schematic graph of the microwave heating system.

loss rate of a water-laden sandstone and extended our previous mathematical model to predict the dynamic phenomena occurring in the sandstone heated by microwaves. The advantage of studying sandstone instead of cotton is that the heat and mass transfer processes are easier to model in the former.

EXPERIMENT

Sample Preparation and Characterization

The sample studied is a cylindrical sandstone 17.4 cm long and 5 cm in diameter. Sample preparation and the measurements of the porosity, capillary pressure, and permeability of the sandstone are detailed elsewhere (Wei et al., 1984). The dielectric constants and loss tangents at various saturations were measured at MIT by W. B. Westphal using a standing-wave method with shorted samples. The general technique is described by Nelson et al. (1972).

Drying Experiments

The heating system, whose schematic layout is depicted in Figure 1, is a specially constructed hybrid microwave-convection oven with controllable microwave power at 2450 MHz, oven temperature, and air flow rate (Hung, 1980). For receiving the water-filled sandstone, the oven was maintained at room temperature with air circulating at 0.245 m/sec. Teflon discs wrapped in aluminum foil were used to cover both ends of the sample, and thermocouples were mounted at three radial positions along the axial direction halfway through the sample. Then, connected to the balance on the top of the oven, the sample was suspended at the center of the oven chamber. After the oven door was secured, the microwave power was turned on and controlled at 60 W. Temperatures were recorded by a multichannel chart recorder, when the microwave power was momentarily turned off. Weight loss was measured with the balance every 5 min for 1 h. Also, the fraction of wet surface was estimated throughout the experiment. The wet fraction is defined as the darker area (wet surface) divided by the sample area.

THEORY

As in our previous model, we shall assume that the porous medium is rigid, that no chemical reactions occur in the sample, and that local thermal equilibrium exists in the sample. One can then derive the following Darcy-level conservation equations (Whitaker, 1977).

Thermal energy equation:

$$\rho C_p \frac{\partial T}{\partial t} + (\rho_\ell C_{p\ell} \bar{v}_\ell + \rho_g C_{pg} \bar{v}_g) \cdot \nabla T + \Delta h_{vap} \dot{m} = \nabla \cdot (\kappa_{eff} \cdot \nabla T) + q_m \quad (1)$$

in which ρC_p is the volume-averaged heat capacity per unit volume; T the local temperature; t the time; ρ_ℓ and ρ_g the liquid and the gas (air-water vapor mixture) densities, respectively; $C_{p\ell}$ and C_{pg} the respective specific heats; $\bar{v}_\ell$ and $\bar{v}_g$ the Darcy-level superficial velocities; Δh_{vap} the heat of vaporization per unit volume; $\dot{m}$ the mass rate of evaporation per unit volume; κ_{eff} the total effective thermal conductivity tensor; and q_m the rate of microwave energy absorbed per unit volume.

Liquid phase continuity equation:

$$\frac{\partial}{\partial t}(\epsilon_\ell \rho_\ell) + \nabla \cdot (\rho_\ell \bar{v}_\ell) + \dot{m} = 0 \quad (2)$$

where ϵ_ℓ is the liquid volume fraction.

Gas phase continuity equation:

$$\frac{\partial}{\partial t}(\epsilon_g \rho_g) + \nabla \cdot (\rho_g \bar{v}_g) = \dot{m} \quad (3)$$

where ϵ_g is the gas volume fraction.

Gas phase diffusion equation:

$$\frac{\partial}{\partial t}(\epsilon_g \rho_a) + \nabla \cdot (\rho_a \bar{v}_g) = \nabla \cdot [\rho_g \boldsymbol{D}_{eff,a} \cdot \nabla(\rho_a / \rho_g)] \quad (4)$$

where ρ_a is the air density, and $\boldsymbol{D}_{eff,a}$ is the effective diffusion tensor of air in the air-water vapor mixture. Although these formulas are valid for anisotropic porous media, we use only their isotropic limits in the analysis given below.

Liquid in a drying porous medium exists in either isolated or accessible states. Accessible liquid is connected by a continuous path to the sample surface and therefore can deliver moisture to the sample surface by liquid convection, a process much more effective for moisture release than vaporization followed by gaseous diffusion and convection, the process whereby isolated liquid must deliver moisture to the surface.

As in our previous work, we express Darcy's law for liquid in the form

$$\bar{v}_\ell = -(\boldsymbol{K}_\ell / \mu_\ell) \cdot [\nabla P_g + k_\epsilon \nabla \epsilon_\ell + k_T \nabla T - \rho_\ell g] \quad (5)$$

in which $k_\epsilon = -\partial P_c(\epsilon_\ell, T)/\partial \epsilon_\ell$ and $k_T = -\partial P_c(\epsilon_\ell, T)/\partial T$. Also, in Eq. 5, $\boldsymbol{K}_\ell$ and μ_ℓ denote the permeability tensor and the liquid viscosity, respectively, and P_g the gas pressure.

The appropriate version of Darcy's law for the gas phase is

$$\bar{v}_g = -(\boldsymbol{K}_g / \mu_g) \cdot [\nabla P_g - \rho_g g] \quad (6)$$

where $\mathbf{K}_g$ and μ_g are the permeability tensor and the gas viscosity, respectively.

With the assumption of local thermal equilibrium, Kelvin's equation can be used to calculate the density of water vapor in the temperature and pressure range of interest here (Collins, 1961):

$$\rho_v = \rho_{v,sat} \exp(-P_c \tilde{V}_\ell / R_g T) \quad (7)$$

where ρ_v is the water vapor density and $\rho_{v,satd}$ represents the saturated water vapor density at temperature T; and $\tilde{V}_\ell$ and R_g are the liquid molar volume and gas constant, respectively.

Microwave heating is volumetric in nature. If a dielectric sample is placed in a high frequency electromagnetic field, local dipole moments attempt to align with the rapidly changing alternating-current field. Because of intermolecular friction, the electrical energy injected into the dipoles is partly dissipated into the medium and causes heating of the sample. Thus, the sample absorbs microwave power. According to Lambert's law (von Hippel, 1954; Mudgett, 1982), the power absorbed per unit volume in a long cylinder of radius R can be expressed as

$$q_m(r) = q_m(R) e^{-2(R-r)/\delta} \quad (8)$$

where $q_m(r)$ is the power absorbed per unit volume at a distance $(R - r)$ from the surface; r the radial position; and δ the characteristic penetration depth, which is the distance through which the electric field strength decays to $1/e$ of its original value. The characteristic penetration depth can be calculated from

$$\delta = \frac{\lambda}{\pi} \left[\frac{1}{2D(\sqrt{1 + \tan^2\theta} - 1)} \right]^{1/2} \quad (9)$$

in which λ is the wavelength of microwaves in free space; D the dielectric constant relative to vacuum; and $\tan\theta$ the loss tangent.

TABLE 1. DIELECTRIC PROPERTIES OF THE WATER-LADEN SANDSTONE

Liquid Saturation, $\epsilon_\ell/(\epsilon_\ell+\epsilon_g)$	Dielectric Constant, D	Loss Tangent, $\tan\theta$	Characteristic Penetration Depth, δ, cm
0	3.72	6.34×10^{-3}	318.69
0.05	4.04	5.53×10^{-2}	35.07
0.42	6.93	8.39×10^{-2}	17.66
0.58	8.0	9.5×10^{-2}	14.44
0.62	8.45	9.6×10^{-2}	13.98
0.82	10.07	0.11	10.91
0.92	10.86	0.1303	9.09
1.0	11.33	0.1323	8.77

The proper initial conditions for the experiment considered are

$$\epsilon_\ell(t=0,r)=\epsilon_{\ell i},\ P_g(t=0,r)=P_{\text{atm}},\text{ and } T(t=0,r)=T_i \tag{10}$$

Besides the symmetry condition applied at the center of the sample, three surface boundary conditions are imposed. The first one is the thermal condition:

$$h(T-T_r)n+\Delta h_{\text{vap}}A_{\text{eff}}M_w N_{vs}=-\kappa_{\text{eff}}\cdot\nabla T \tag{11}$$

where h is the heat transfer coefficient; n the unit outer normal vector to the sample surface; A_{eff} the fraction of wet surface; M_w the molecular weight of water; and N_{vs} the molar flux of water vapor at surface. The second surface boundary condition is for liquid moisture:

$$\rho_\ell\bar{v}_\ell=A_{eff}M_w N_{vs}+\rho_v\bar{v}_g+\rho_g D_{\text{eff},a}\cdot\nabla(\rho_a/\rho_g) \tag{12}$$

The third boundary condition is that the gas pressure at the surface is 1 atm.

SOURCES OF PHYSICAL PROPERTIES

Except for the heat and mass transfer coefficients h and k_x, the physical properties of the sandstone are taken from the Table 1 of our previous paper (Wei et al., 1984). The coefficients h and k_x were not measured but instead were estimated from limited drying

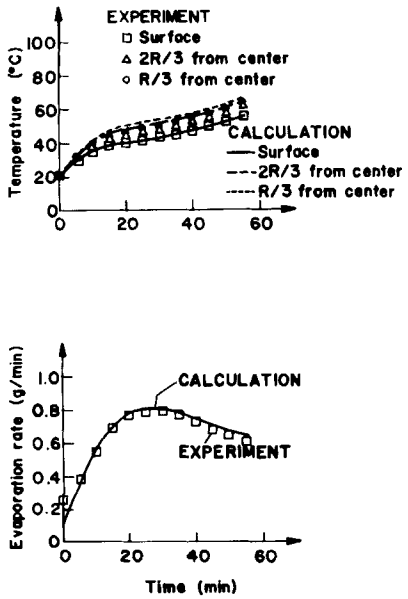

Figure 2. The histograms of temperatures and evaporation rate for sandstone.

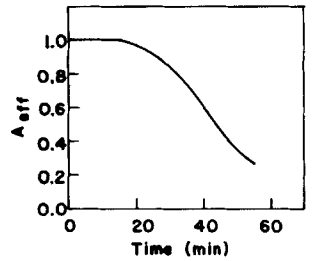

Figure 3. The fraction of wet surface area versus time.

data. We estimated k_x from film theory (Bird et al., 1960), according to which

$$1+\frac{x_{wo}-x_{w\infty}}{\dfrac{N_{wo}}{N_{wo}+N_{ao}}-x_{wo}}=\exp\left[\frac{N_{wo}-N_{ao}}{k_x}\right], \tag{13}$$

where x_{wo} and $x_{w\infty}$ are the mole fraction of water vapor at the wet sample surface and in the drying medium, and N_{wo} and N_{ao} are the flux of water vapor and air at the sample surface. For the experiments reported here air flux was negligible. The flux of water was computed as the rate of water lost by the sample divided by the exposed area of the sample. We calculated k_x using data taken at three different times. The values found were within a few percent of one another and so their average value, $k_x=0.5$ mole/m^2-s was accepted as correct for the microwave heating. The heat transfer coefficient, h, was calculated from the boundary flux balance, Eq. 11, with data taken at the same times as those used to calculate the mass transfer coefficient. Again the three values were within a few percent of one another and the average value, $h=16.7$ W/m^2 K, was accepted as correct.

The dielectric constants, loss tangents, and characteristic penetration depths at various liquid saturations are listed in Table 1.

NUMERICAL ANALYSIS

A one-dimensional model was employed in the analysis since the sample approximates an infinite cylinder with both ends covered by aluminum foil. The backward-difference implicit method and the six-point orthogonal collocation method were used to solve the nonlinear differential equations. The computational schemes are presented elsewhere (Wei et al., 1984). For this case, the computing time for the implicit scheme is 698 s with a spatial mesh 0.0625 cm

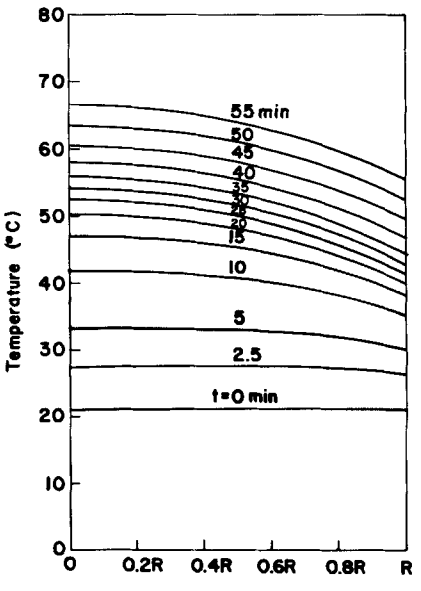

Figure 4. History of temperature profile.

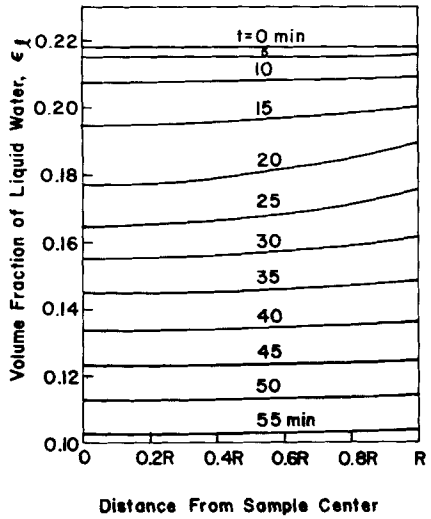

Figure 5. History of liquid saturation distribution.

and a time step 0.75 sec on a CYBER 74 computer. The computing time for the orthogonal collocation method is 85 s with the same time step. The two sets of solutions agree and will be discussed in the next section.

RESULTS AND DISCUSSION

During the microwave heating process, the sandstone surface was totally wet in the first 15 min; thereafter dry spots start to appear. As characterized by Figure 3, the specific effective area for evaporation gradually decreased with time. In Figure 2, experimental water loss rates and temperatures are plotted and compared with predictions of the theoretical model. The experimental and theoretical curves agree quite well.

In Figures 4–8 are the predicted distributions of temperature, liquid content, vapor density, air density, and gas pressure within the cylindrical sandstone at selected time levels. In contrast to that in convective heating, the microwave-heated sample is hotter inside, as indicated in Figure 4. The calculated temperatures in the cylinder rise up rapidly in the beginning, slow down in the middle, and increase again moderately by the end of the heating period. This is mainly due to surface evaporation: A large portion of the internally absorbed microwave energy is convected by liquid to the surface where it evaporates and cools the surface; the rate of microwave energy absorbed is approximately constant, the surface cooling increases monotonically with time, and the evaporation rate increases in the beginning and then decreases.

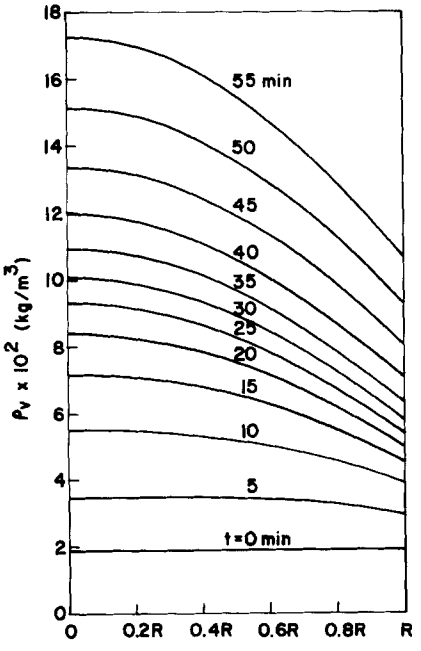

Figure 6. History of vapor density profile.

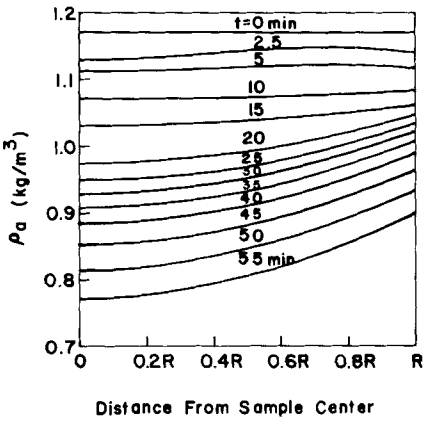

Figure 7. History of air density profile.

Figure 5 is the theoretical histogram of liquid moisture distribution. Unlike the profiles of liquid volume fraction in convectively heated sandstone, here the liquid volume fraction at any instant increases slightly with distance toward the surface, and at any position the liquid volume fraction declines steadily with time; this behavior is similar to the experimental results found for cotton in the work of Lyons and Hatcher (1972), although their heating intensity may have been higher than ours.

The vapor density profiles and the air density profiles at several time levels are depicted in Figures 6 and 7, respectively. Due to thermal equilibrium, the vapor density varies more sharply with distance than does temperature because the density of equilibrated vapor increases exponentially with temperature. The sharpness of the vapor density profile grows with time and causes an increase in the diffusive vapor flux to the surface. On the other hand, air density at any point in the sample gradually decreases due to increase of void (gas) volume and slow air supply.

The progressive pressure distribution in the gas phase within the cylinder is shown in Figure 8. In the beginning, a ring of maximum pressure shrinks to the sample's axis while the pressure is rising. Then the ring becomes a centered pressure peak and the pressure

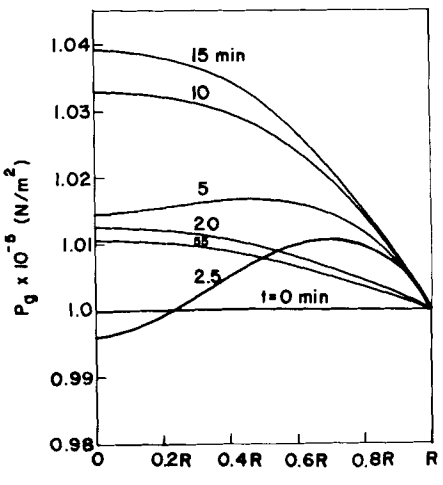

Figure 8. History of gas pressure distribution.

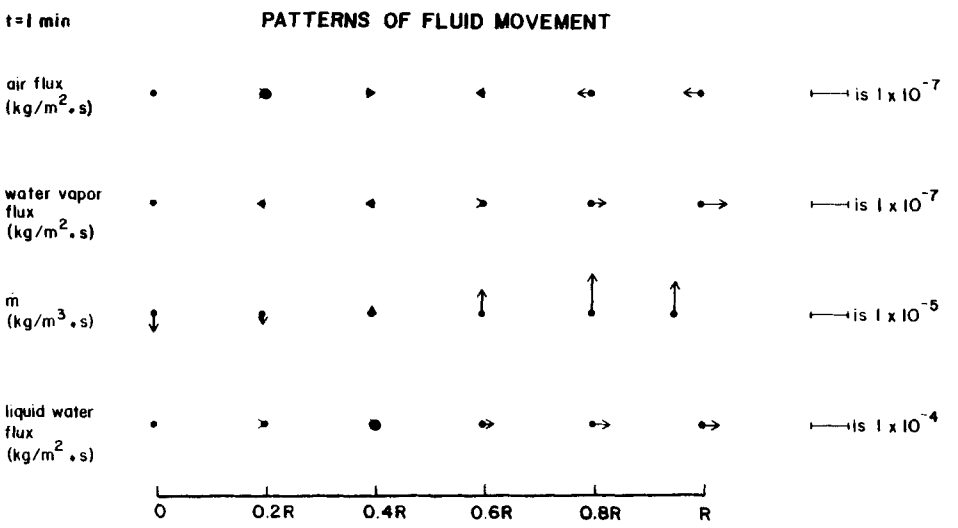

Figure 9. Fluid flow pattern at 1 min.

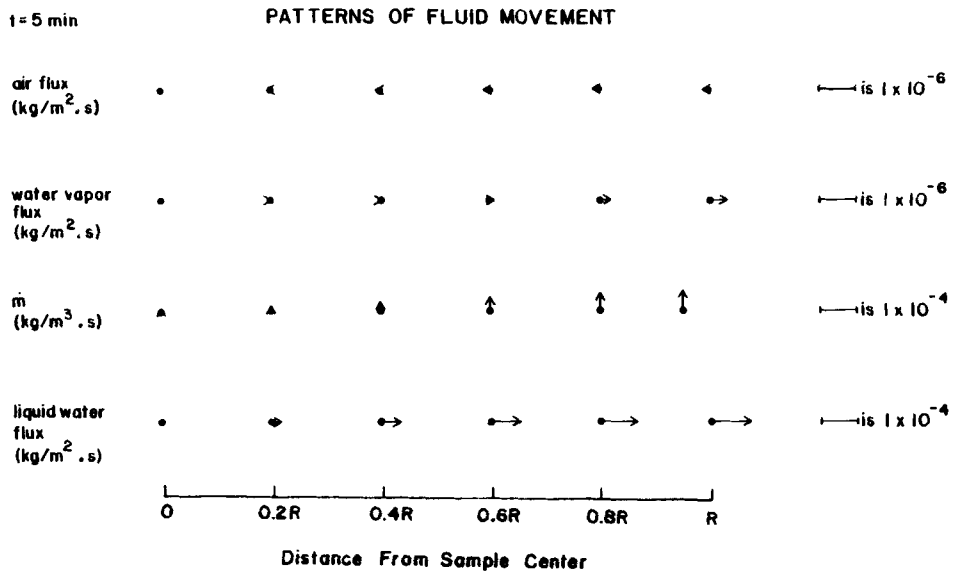

Figure 10. Fluid flow pattern at 5 min.

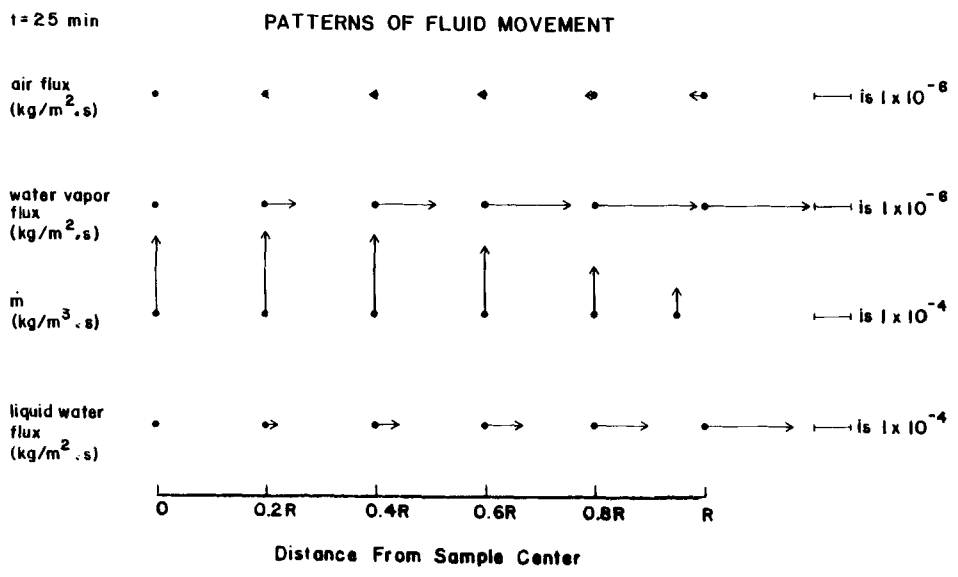

Figure 11. Fluid flow pattern at 25 min.

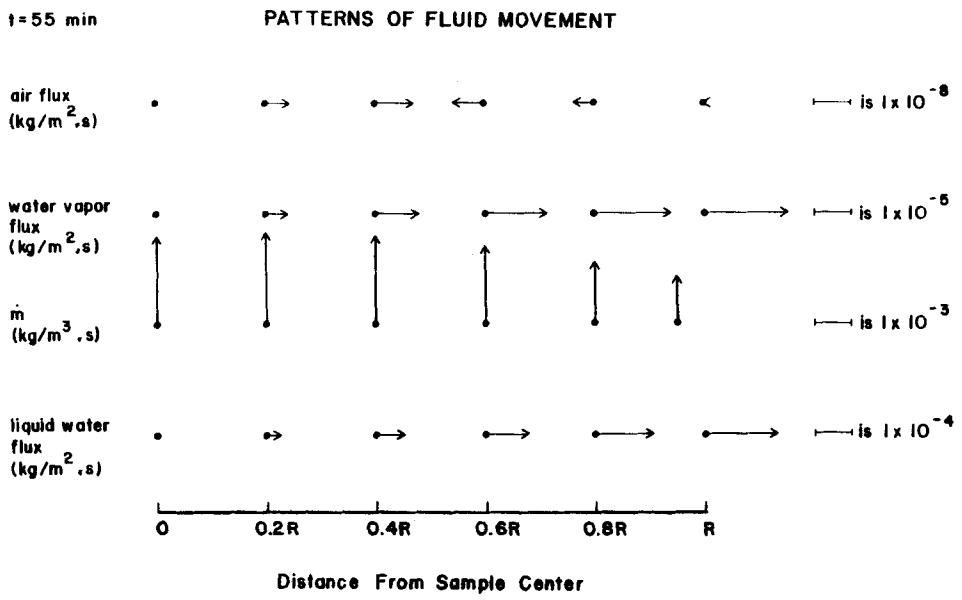

Figure 12. Fluid flow pattern at 55 min.

keeps going up. After the peak reaches the highest pressure at about 15 min, the pressure starts falling. This transition behavior in the pressure peak was also reported by Lyons and Hatcher (1972).

The fluid flow patterns in the sandstone at 1, 5, 25, and 55 min are shown diagrammatically in Figures 9–12, respectively. Although there exist different flow patterns during the first few minutes, during most of the heating period air slowly flows to the sample's center, water vapor flows to the surface, and liquid vaporizes as it flows to the surface with higher flux than vapor. Interestingly, liquid driven by pressure gradient flows in the direction of increasing saturation. Detailed calculations show that vapor diffusion is enhanced by convective vapor flow, but air diffusion is retarded by convective air flow; therefore vapor flux is larger than air flux. Figure 13 summarizes in a more conventional plot the flow patterns depicted in Figures 9–12.

As a final remark, the major objectives of our previous study and this work are to investigate the fluid flow and heat transfer phenomena in a rigid, disordered porous medium and to explain the drying mechanisms in external or internal heating. Further research on boundary phenomena during drying will help to predict drying characteristic curves more accurately.

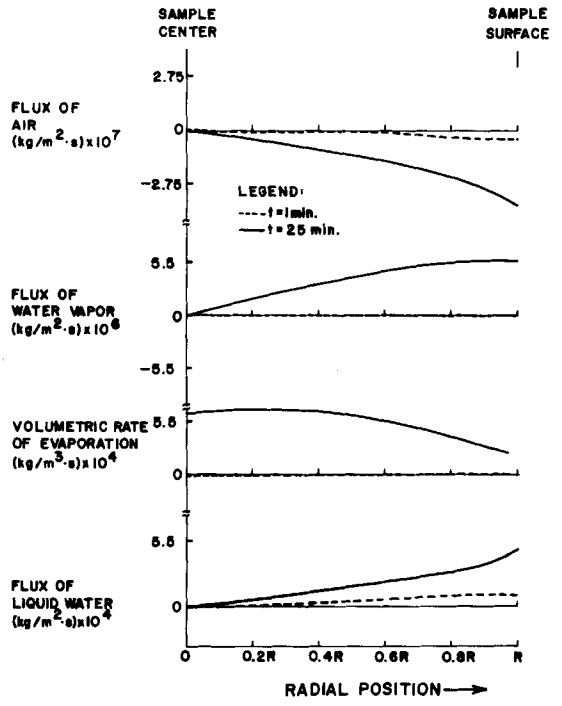

Figure 13. Profiles of predicted fluid fluxes at 1 and 25 min.

ACKNOWLEDGMENT

Paper No. 14,489 Scientific Journal Series, Minnesota Agricultural Experimental Station, St. Paul, MN 55108. Projects 18-027 and 18-063. We acknowledge W. B. Westphal of the Department of Electrical Engineering and Computer Science of MIT for his measurement of the dielectric properties of the sandstone. We are grateful to the University of Minnesota Computer Center for a grant to support the computations reported here.

NOTATION

A_{eff} = fraction of wet surface
C_p = mass fraction weighted average constant pressure heat capacity, J/kg·K
$C_{p\ell}$, C_{pg} = constant pressure heat capacity of liquid, vapor. J/kg·K
$D_{\text{eff},a}$ = total efffective diffusivity tensor of air in airwater vapor mixture, m^2 /s
D = dielectric constant relative to vacuum
g = gravity vector, m/s^2
h = heat transfer coefficient, W/m^2·K
Δh_{vap} = enthalpy of vaporization per unit mass, J/kg
K = permeability tensor, μm^2
k_ϵ = $-\partial P_c(\epsilon_\ell, T)/\partial \epsilon_\ell$, N/m^2
k_T = $-\partial P_c(\epsilon_\ell, T)/\partial T$, N/m_2·K
k_x = mass transfer coefficient, mol/m^2·s
M_w = molecular weight of water, kg/mol
$\dot{m}$ = mass rate of evaporation per unit volume, kg/m^3·s
N_{vs} = molar flux of water vapor at surface, mol/m^2·s
n = unit outer normal vector to surface
P_{atm} = atmospheric pressure, N/m^2
P_c = capillary pressure, N/m^2
P = pressure, N/m^2
q_m = rate of microwave energy absorbed per unit volume, W/m^3
R = radius, cm
R_g = gas constant, J/mol·K
r = radial coordinates, cm

T_c = critical temperature of water, K
T_r = room temperature, K
T = temperature, K
t = time, s
$\tan\theta$ = loss tangent
V_ℓ = molar volume of liquid water, m^3/mol
$\bar{v}$ = local superficial velocity, m/s
x = mole fraction

Greek Letters

δ = characteristic penetration depth of microwave energy, m
ϵ = volume fraction
κ_{eff} = total thermal conductivity tensor, m^2/s
λ = wavelength of microwaves in free space, m
μ = viscosity, kg/m·s
ρ = density, kg/m^3

Subscripts

a = property of air
g = property of gas phase
i = initial condition
ℓ = property of liquid water
v = property of water vapor

LITERATURE CITED

Bird, R. B., W. E. Stewart, and E. N. Lightfoot, *Transport Phenomena*, Wiley, New York (1960), p. 662.

Hung, C. C., "Water Migration and Structural Transformation of Oven Cooked Meat," Ph.D. Thesis, Univ. of Minnesota (1980).

Lyons, D. W., and J. D. Hatcher, "Drying of a Porous Medium with Internal Heat Generation," *Int. J. Heat Mass Transfer*, **15**, 897 (1972).

Mudgett, R. E., "Electrical Properties of Foods in Microwave Processing," *Food Technol.*, 109 (Feb. 1982).

Nelson, S. O., C. W. Schlaphoff, and L. E. Stetson, "Computer Program for Calculating Dielectric Properties of Low- or High-Loss Materials from Short-Circuited Waveguide Measurements," U.S. Department of Agriculture ARS-NC-4 (Nov., 1972).

von Hippel, A. R., *Dielectrics and Waves*, Wiley, New York, 9 (1954).

Watanabe, M., M. Suzuki, and S. Ohkawa, "Analysis of Power Density Distribution in Microwave Ovens," *J. Microwave Power*, **13**(2), 173 (1978).

Wei, C. K., H. T. Davis, E. A. Davis, and J. Gordon, "Heat and Mass Transfer in Water-Laden Sandstone: Convective Heating," *AIChE J.*, accepted for publication.

Whitaker, S., "Simultaneous Heat, Mass and Momentum Transfer in Porous Media: A Theory of Drying," *Adv. Heat Transfer*, **13**, 119 (1977).

Manuscript received Mar. 14, 1984; revision received June 1, and accepted June 3.